Effect of half-space and interface phonons on the transport properties of $Al_xGa_{1-x}As/GaAs$ single heterostructures

Paolo Bordone*
Dipartimento di Fisica ed Istituto Nazionale di Fisica della Materia, Università di Modena, Via Campi 213/A, 41100 Modena, Italy

Paolo Lugli
Dipartimento di Ingegneria Elettronica, Università di Roma Tor Vergata, Via della Ricerca Scientifica, 00133 Roma, Italy

(Received 14 May 1993)

We present a detailed analysis of the influence of the various phonon modes characteristic of the single heterostructure $Al_xGa_{1-x}As/GaAs$ on its electronic transport by using a Monte Carlo simulation. The electronic states of the system are calculated by solving self-consistently the coupled Schrödinger-Poisson equations for the system. LO-phonon states are treated within the dielectric continuum model by using two different dielectric functions to describe the two semiconductors, the usual Lyddane-Sachs-Teller expression for GaAs and a generalized two poles expression for $Al_xGa_{1-x}As$. Two sets of optical modes characterize the system, the half-space LO modes and the interface modes. The scattering rates for the interaction of these modes with the confined electrons are calculated from the Fermi golden rule. A Monte Carlo simulation is then used to study the effect of the electron-phonon interaction on the transport properties of a single $Al_xGa_{1-x}As/GaAs$ heterostructure in the presence of an electric field applied along the heterointerface. The results of simulations performed at 300 and 77 K compare favorably with available experimental data. Drag and heating effects related to nonequilibrium phonon effects are found and discussed.

I. INTRODUCTION

Heterostructures have achieved a relevant role in recent years in the microelectronics field, as they have brought an improvement in the transport properties of electronic devices[1] and the modulation properties of optoelectronic devices.[2] In two-dimensional structures, high mobility has been achieved thanks to the modulation doping technique, which was first applied by Dingle *et al.*[3] and Störmer[4] to $Al_xGa_{1-x}As/GaAs$ heterostructures. The idea of selective doping of semiconductor heterostructures is very simple and very powerful. During the growth of the epitaxial layer a dopant is added only in the barrier material (wider gap material), while the well material (GaAs in our case) is grown as pure as possible. Thus a spontaneous and irreversible charge transfer into the narrow-gap material is induced. The spatial separation between the electrons and their parent donors has important consequences. Electrons are confined in a quasitriangular well near the interface formed because band bending taking place due to the dipole formed between the positive (ionized donors) and the negative (electrons) charges. Bound states are formed which force the carrier motion to be effectively quasi-two-dimensional. The free-electron motion along the heterointerface is characterized by a very high mobility caused by the spatial separation between the carriers and the parent donors.[5]

Modulation doping is useful to increase the electron mobility at low temperature, where the scattering between carriers and ionized impurities is the most relevant mechanism, but becomes much less important at room temperature, where the interaction with phonons is dominant. The presence of the heterointerface does indeed modify the vibrational properties of the lattice, but the influence of this modification on the carrier transport properties has never been studied.

In this paper, we analyze the transport properties of an $Al_xGa_{1-x}As/GaAs$ single heterostructure using a Monte Carlo (MC) method, focusing in particular on the polar interaction between electrons and phonons. The electronic transport in this system has already been studied using a MC code by Yokoyama and Hess,[6] who accounted for size quantization by solving the coupled Schrödinger-Poisson equations, and considered bulklike phonons in the calculation of the scattering rates. Here we account for electron size quantization in a similar way (considering both Γ and L valleys) and consider explicitly the two-dimensional properties of the phonon spectra by adopting a dielectric continuum model (DCM).[7-9] The validity of the DCM in describing optical modes of heterostructures has been proven by Rücker, Molinari, and Lugli[10] through a comparison with a microscopic phonon model. We use two different dielectric functions to describe the two layers, the usual Lyddane-Sachs-Teller expression for GaAs, and a generalized two poles expression for $Al_xGa_{1-x}As$ (Ref. 11) which depends on the Al composition of the alloy. The phonon frequencies and displacements are used to calculate the electron-phonon-scattering rates which, in turn, enter the MC calculation of the heterostructures-transport properties. This paper is organized as follows. In Sec. II, the self-consistent calculation of the electronic states of the quasitriangular well is presented. The energy levels and the correspond-

0163-1829/94/49(12)/8178(13)/$06.00 ©1994 The American Physical Society

ing wave functions are evaluated numerically. In Sec. III we calculate the modes characteristic of the $Al_xGa_{1-x}As/GaAs$ single heterostructure by using a dielectric continuum model and a two poles dielectric function for the alloy. Results of Secs. II and III are used to calculate the electron-phonon-scattering probabilities in Sec. IV. Transport properties of an $Al_xGa_{1-x}As/GaAs$ single heterostructure as studied by our MC simulation are presented in Sec. V, focusing in particular on the contribution of the different modes characteristic of the system, and on the role of nonequilibrium phonons.[12–14]

II. SELF-CONSISTENT CALCULATION OF ENERGY LEVELS AND WAVE FUNCTIONS IN A SINGLE HETEROJUNCTION

The electronic level wave functions in the single $Al_xGa_{1-x}As/GaAs$ heterostructure described by a self-consistent potential $\Phi_{\text{s.c.}}$ are calculated by solving the coupled Schrödinger and Poisson equations:

$$-\frac{\hbar^2}{2m^*}\frac{d^2\chi_i(z)}{dz^2}+V_b(z)\chi_i(z)-e\Phi_{\text{s.c.}}(z)\chi_i(z)=E_i\chi_i(z)\ , \quad (1)$$

$$\frac{d^2\Phi_{\text{s.c.}}(z)}{dz^2}=\frac{e}{\epsilon_0\epsilon_r}\left[\sum_{i\ \text{occupied}} n_i\chi_i^2(z)+N_A(z)-N_D(z)\right]\ , \quad (2)$$

where m^* is the electron effective mass, V_b is the conduction-band discontinuity at the interface, e is the electron charge, ϵ_r is the static dielectric constant, n_i and χ_i are the number and wave function of electrons in the subband i, and $N_A(z)$ and $N_D(z)$ are the position-dependent acceptor and donor concentrations. At equilibrium, the Fermi energy of the electrons E_F and the quantities n_i, E_i, and m^* are related by the equation

$$n_i=\frac{m^*k_BT}{\pi\hbar^2}\ln\left[1+\exp\left[\frac{E_F-E_i}{k_BT}\right]\right]\ . \quad (3)$$

The solution of the coupled equations is obtained via a standard iterative method[15–18] which starts from an initial guess of the electronic density and energy levels, and evolves until convergence is achieved. We determine the number of valleys to consider, two (Γ and L) in the present case, fix the subband number in each valley, and initialize the subband energies to reasonable values. Two valleys (Γ and L) are considered explicitly, each described in the effective-mass approximation scheme. Within $Al_xGa_{1-x}As$ the effective mass is expressed as a function of the Al composition x according to the following rules: $m_c^\Gamma/m_0=0.067+0.083x$ for the Γ valley, and $m_c^L/m_0=0.11+0.03x$ for the L valley. In this paper we neglect the X-valley contribution. This is a reasonable assumption for an Al composition $x\leq 0.35$ (Ref. 19) and moderate electric field values ($E\leq 5$ kV/cm).

Figure 1(a) shows the potential shape for both Γ and L valleys, at 300-K temperature, for an Al composition

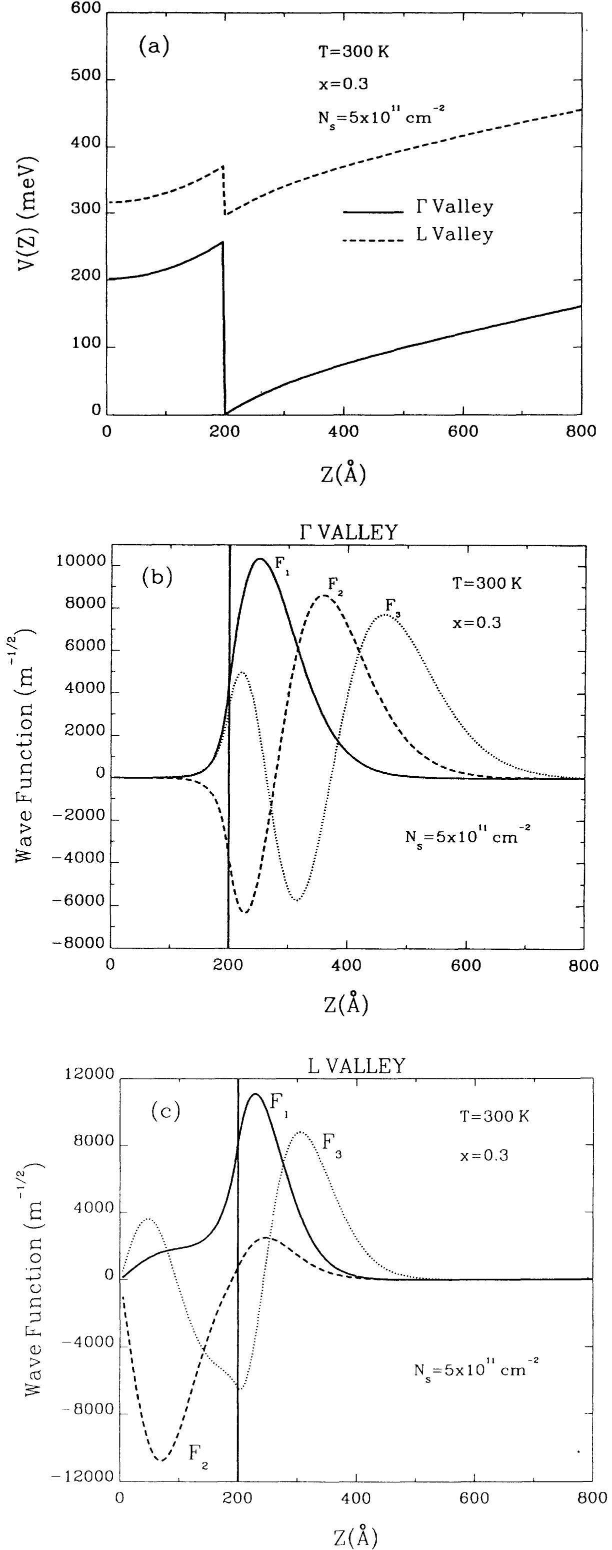

FIG. 1. (a) Calculated effective potential for Γ and L valleys at a 300-K lattice temperature, for an Al composition $x=0.3$ and a bidimensional electron-gas concentration $N_S=5\times10^{11}$ cm^{-2}. The $Al_{0.3}Ga_{0.7}As$ barrier region is doped with a donor concentrations $N_D=5\times10^{17}$ cm^{-3}, while the GaAs region is intrinsic. (b) Calculated wave functions for the three lowest subbands in the Γ valley corresponding to (a). (c) Same as (b) but for the L valley.

$x=0.3$ and a surface carrier density $N_s=5\times10^{11}$ cm^{-2}. The $Al_{0.3}Ga_{0.7}As$ region is doped with a donor concentration $N_D=5\times10^{11}$ cm^{-2}, while the GaAs is assumed to be intrinsic. Figures 1(b) and 1(c) report wave functions corresponding to the first three subbands of the Γ and L valleys, respectively. At the present Al composition the conduction-band discontinuity between the two semiconductors is 256 meV in Γ and 75 meV in L. In the Γ valley, the electron wave function penetrates only slightly in the alloy. In the ground state electrons are localized within about 200 Å from the interface, while for higher-energy levels the degree of carrier localization decreases. Things change drastically in the L valley, where the much lower potential barrier allows strong penetration of the wave functions in the $Al_xGa_{1-x}As$ region. We have in this case a strongly coupled system, in which the wave function of the first level is localized in the GaAs well while the other are mainly localized in the $Al_xGa_{1-x}As$ barrier. Therefore we cannot properly speak of carrier confinement for L-valley electrons.

III. DIELECTRIC CONTINUUM MODEL

Within the dielectric continuum approach,[7-9] the vibrational properties of a given structure are determined from the following set of equations:

$$\nabla^2\Phi(\mathbf{R})=\frac{1}{\epsilon_0}\nabla\cdot\mathbf{P}(\mathbf{R}) , \quad (4)$$

$$\mathbf{P}(\mathbf{R})=\epsilon_0\chi_n(\omega)\mathbf{E}(\mathbf{R}) , \quad (5)$$

$$\mathbf{E}(\mathbf{R})=-\nabla\Phi(\mathbf{R}) , \quad (6)$$

$\mathbf{P}(\mathbf{R})$ is the polarization field, $\mathbf{E}(\mathbf{R})$ is the electric field, $\chi_n(\omega)=\epsilon_n(\omega)-1$ is the dielectric susceptibility in the nth layer, and $\Phi(\mathbf{r})$ is the electrostatic potential of the optical-phonon modes, which can be factorized as

$$\Phi(\mathbf{R},t)=\phi(z)e^{i(\mathbf{q}\cdot\mathbf{r}-\omega t)} , \quad (7)$$

where $\mathbf{q}$ and $\mathbf{r}$, respectively, are the components of the phonon wave vector and of the position vector parallel to the interface.

In the case of an $Al_xGa_{1-x}As$/GaAs single heterostructure, the dielectric functions in GaAs and $Al_xGa_{1-x}As$ are given, following the generalized Lyddane-Sachs-Teller relation, as

$$\epsilon_1(\omega)=\epsilon_{\infty 1}\frac{(\omega^2-\omega_{L1}^2)}{(\omega^2-\omega_{T1}^2)} , \quad (8)$$

$$\epsilon_2(\omega)=\epsilon_{\infty 2}\frac{(\omega^2-\omega_{L2A}^2)(\omega^2-\omega_{L2G}^2)}{(\omega^2-\omega_{T2A}^2)(\omega^2-\omega_{T2G}^2)} , \quad (9)$$

where the subscripts 1 and 2 are for the GaAs and $Al_xGa_{1-x}As$ regions, respectively, and L represents the LO and T the TO phonon modes, respectively. The two-mode behavior of the ternary semiconductor in Eq. (9) is evidenced by the subscripts A and G, which stand for AlAs- and GaAs-like modes, respectively.[11] The two poles dielectric function behavior is reported in Fig. 2. In the diatomic binary semiconductor (GaAs) the equation of motion, within the continuum approximation, is

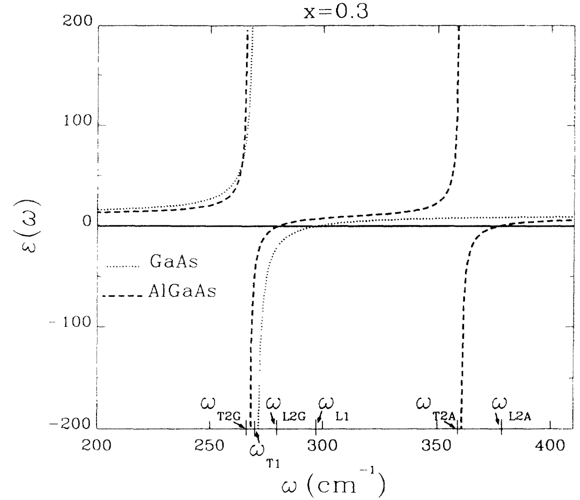

FIG. 2. Two poles dielectric function, used to describe the ternary semiconductor.

$$-\mu_1\omega^2\mathbf{u}(\mathbf{R})=-\mu_1\omega_{01}^2\mathbf{u}(\mathbf{R})+e_1^*\mathbf{E}^{\rm loc}(\mathbf{R}) \quad (10)$$

and the polarization microscopic expression is

$$\mathbf{P}(\mathbf{R})=n_1e_1^*\mathbf{u}(\mathbf{R})+n_1\alpha_1\mathbf{E}^{\rm loc}(\mathbf{R}) , \quad (11)$$

where $\mathbf{u}(\mathbf{r})$ is the relative displacement of an ion pair, μ_1 is the reduced mass of an ion pair, ω_{01} is the frequency associated with the short-range forces between ions, e_1^* is the effective charge of a unit cell, n_1 is the number of unit cells per unit volume, α_1 is the electronic polarizability per unit cell, and the local electric field $\mathbf{E}^{\rm loc}=\mathbf{E}+\mathbf{P}/3\epsilon_0$.

In the ternary semiconductor the relative motion in a unit cell can take two different characteristic equations of motion, one GaAs-like and one AlAs-like:

$$-\mu_{2i}\omega^2\mathbf{u}_m(\mathbf{R})=-\mu_{2i}\omega_{02i}^2\mathbf{u}_m(\mathbf{R})+e_{2i}^*\mathbf{E}^{\rm loc}(\mathbf{R}) , \quad i=A,G \quad (12)$$

and, as a result, the polarization field can be approximated to the first order in the material composition x, as

$$\mathbf{P}(\mathbf{R})=n_2[xe_{2A}^*\mathbf{u}_A(\mathbf{R})+(1-x)e_{2G}^*\mathbf{u}_G(\mathbf{R})] +n_2\alpha_2\mathbf{E}^{\rm loc}(\mathbf{R}) . \quad (13)$$

The normal mode frequencies and the corresponding $\Phi(\mathbf{R})$, $\mathbf{P}(\mathbf{R})$, and $\mathbf{E}(\mathbf{R})$ can be obtained by solving Eqs. (5)–(13) together with the appropriate electrostatic boundary conditions at the interface.[11]

For the z component of the phonon potential, we have

$$\phi_1(z)=\phi_2(z) \quad (14)$$

and

$$\epsilon_1(\omega)\frac{d\phi_1(z)}{dz}=\epsilon_2(\omega)\frac{d\phi_2(z)}{dz} , \quad (15)$$

which are derived by imposing the continuity of the in-plane electric field and of the transversal electric displacement. Equations (14) and (15) lead to two sets of modes: *interface modes,* if both $\epsilon_1(\omega)$ and $\epsilon_2(\omega)$ are different from zero, with

$$\phi(z)=\begin{cases} Ae^{-qz} & z>0, \quad \text{GaAs} \\ Be^{qz} & z<0, \quad \text{Al}_x\text{Ga}_{1-x}\text{As} , \end{cases} \tag{16}$$

and *half-space LO modes* [whose potential goes like $\sin(q_z z)$] if one of the two dielectric functions is zero. The frequencies of the interface modes are given by the solution of the equation

$$\epsilon_1(\omega)+\epsilon_2(\omega)=0 . \tag{17}$$

With $\epsilon_{1,2}(\omega)$ given by Eqs. (8) and (9), Eq. (17) is a third-degree equation in ω, with three real and distinct solutions which give the three interface normal mode frequencies: ω_1 originating from the GaAs modes of the GaAs region; and ω_2 and ω_3 originating from the AlAs-like modes and the GaAs-like modes, respectively, of the $\text{Al}_x\text{Ga}_{1-x}\text{As}$ region.[11] Figures 3(a) and 3(b) show the spatial dispersion of the interface (dashed line) and half-space LO modes (dotted line and dashed-dotted line), for two different values of q and q_z. Here the origin is fixed at the interface plane.

The two-dimensional Fourier transform $\Phi(\mathbf{q},z)$ of the phonon potential $\Phi(\mathbf{R})$ determines the electron-optical-phonon interaction Hamiltonian, which is given, for each normal mode, by[9,11,20,21]

$$H_{\text{ep}}=\sum_{\mathbf{q}} -e\Phi(\mathbf{q},z)e^{i\mathbf{q}\cdot\mathbf{r}}\left[\frac{\hbar}{2\omega}\right](\hat{a}_{\mathbf{q}}+\hat{a}^{+}_{-\mathbf{q}}) , \tag{18}$$

where $\hat{a}$ and $\hat{a}^{+}$ are the usual annihilation and creation operators. For the interface modes, the interaction Hamiltonian can be written as[11]

$$H_{\text{ep}I}=\sum_{\mathbf{q}}\left[\frac{\hbar e^2L^{-2}}{\epsilon_0 C_I(\omega)}\right]^{1/2}\frac{1}{\sqrt{q}}e^{-q|z|}e^{i\mathbf{q}\cdot\mathbf{r}}(\hat{a}_{\mathbf{q}}+\hat{a}^{+}_{-\mathbf{q}}) , \tag{19}$$

where L^2 is the interface area, and $C_I(\omega)=(\partial/\partial\omega)[\epsilon_1(\omega)+\epsilon_2(\omega)]$.

The Hamiltonian for the half-space LO modes is given by[9]

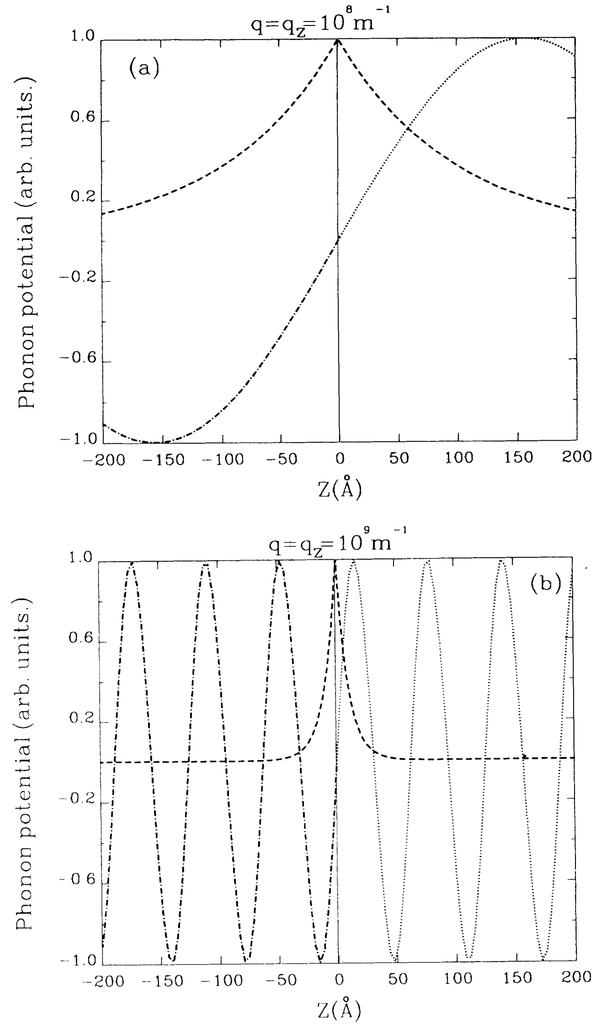

FIG. 3. (a) Phonon potential as a function of position for interface (dashed line) and half-space LO modes (dotted line and dashed-dotted line). Interface modes are evaluated at an in-plane phonon wave vector $q=10^8\ \text{m}^{-1}$, and half-space LO modes at a perpendicular phonon wave vector $q_z=10^8\ \text{m}^{-1}$. The interface is at $z=0$. (b) Same as (a) for $q=q_z=10^9\ \text{m}^{-1}$.

$$H_{\text{ep},1}=-\sum_{q_x>0}\sum_{\mathbf{q}}\left[\frac{\hbar e^2\omega_{L1}}{2\epsilon_0 L^3}\right]^{1/2}\left[\frac{1}{\epsilon_{\infty 1}}-\frac{1}{\epsilon_1(0)}\right]^{1/2}\frac{e^{i\mathbf{q}\cdot\mathbf{r}}}{\sqrt{q^2+q_z^2}}2\sin(q_z z)[\hat{a}_{1,q_z}(\mathbf{q})+\hat{a}^{+}_{1,q_z}(-\mathbf{q})] \tag{20}$$

for the binary material, and by

$$H_{\text{ep},2}=-\sum_{q_z>0}\sum_{\mathbf{q}}\left[\frac{\hbar e^2}{\epsilon_0 L^3}\right]^{1/2}(C_2(\omega))^{1/2}\frac{e^{i\mathbf{q}\cdot\mathbf{r}}}{\sqrt{q^2+q_z^2}}\times 2\sin(q_z z)[\hat{a}_{2,q_z}(\mathbf{q})+\hat{a}^{+}_{2,q_z}(-\mathbf{q})] \tag{21}$$

for the ternary one,[11] where $C_2(\omega)=\partial\epsilon_2(\omega)/\partial\omega$. Here L^3 is the volume of the heterostructure, ω_{L1} is the frequency of the LO phonons in GaAs, and $\epsilon_{\infty 1}$ and $\epsilon_1(0)$ are the optical and static dielectric constants. No phonon dispersion is considered for these modes.

IV. ELECTRON-PHONON INTERACTION

In previous sections we have derived expressions for the electronic wave function, phonon potential, and electron-optical-phonon interaction Hamiltonian, which are all necessary ingredients to evaluate the electron-phonon scattering rate via the *Fermi golden rule:*

$$P(|u\rangle,|u'\rangle)=\frac{2\pi}{\hbar}|\langle u'|H'|u\rangle|^2\delta(E_{u'}-E_u) . \tag{22}$$

Here P describes the probability per unit time for the system to make the transition from an initial state $|u\rangle$ at energy E_u to a final state $|u'\rangle$ at energy $E_{u'}$ under the effect

of a small perturbation, represented by the perturbation Hamiltonian H'.

The transition probability per unit time from an electronic state $\mathbf{K}$ in subband i to an electronic state $\mathbf{K}'$ in subband j is given by

$$P^{I}(\mathbf{K},\mathbf{K}')=\frac{2\pi}{\hbar}\begin{bmatrix} n+1 \\ n \end{bmatrix}\left[\frac{\hbar e^2}{\epsilon_0 L^2 C_I(\omega)}\right]\frac{G^{I}_{ij}(q)}{q}\times\delta\left[\frac{\hbar^2 k'^2}{2m^*}-\frac{\hbar^2 k^2}{2m^*}\pm\hbar\omega^*\right], \quad (23)$$

while the integrated scattering probability is

$$P^{I}_{ij}(\mathbf{K})=\frac{m^* e^2}{2\pi\hbar^2\epsilon_0 C_I(\omega)}\begin{bmatrix} n+1 \\ n \end{bmatrix}\times\int_0^{2\pi}\frac{G^{I}_{ij}(k',\theta)}{\sqrt{k_0'^2+k^2-2kk_0'\cos\theta}}d\theta , \quad (24)$$

where

$$G^{I}_{ij}(q)=\int\chi_j^*(z)\chi_i(z)e^{-q|z|}dz\int\chi_j^*(z')\chi_i(z')e^{-q|z'|}dz'$$

and

$$\pm\hbar\omega^*=\pm\hbar\omega+(E_j-E_i) .$$

In (23) and (24) $q=\sqrt{k_0'^2+k^2-2kk_0'\cos\theta}$ is the component of the phonon wave vector in the interface plane which is obtained from momentum conservation, and the $\pm$ sign refers to the absorption and emission cases, respectively. The calculations of the scattering rates in terms of the electron and phonon states ($|\mathbf{K}\rangle$ and $|n\rangle$, respectively), are reported in Appendix A. The integration over θ is performed numerically.

For the half-space LO phonons, we find (see Appendix B)

$$P^{(1)}(\mathbf{K},\mathbf{K}')=\left[\frac{\pi e^2\omega_{L1}}{\epsilon_0 L^2 q}\right]\left[\frac{1}{\epsilon_{\infty 1}}-\frac{1}{\epsilon_1(0)}\right]\times\begin{bmatrix} n+1 \\ n \end{bmatrix}F^{(1)}_{ij}(q)\times\delta\left[\frac{\hbar^2 k'^2}{2m^*}-\frac{\hbar^2 k^2}{2m^*}\pm\hbar\omega^*\right] \quad (25)$$

and

$$P^{(1)}_{ij}(\mathbf{K})=\left[\frac{\pi e^2\omega_{L1}m^*}{(2\pi)^2\epsilon_0\hbar^2}\right]\left[\frac{1}{\epsilon_{\infty 1}}-\frac{1}{\epsilon_1(0)}\right]\begin{bmatrix} n+1 \\ n \end{bmatrix}\times\int_0^{2\pi}d\theta\frac{F^{(1)}_{ij}(k_0',\theta)}{q} \quad (26)$$

for the GaAs region, where

$$F^{(1)}_{ij}(q)=\int_0^{\infty}\chi_j^*(z)\chi_i(z)dz\times\int_0^{\infty}\chi_j^*(z')\chi_i(z')dz'(e^{-q|z-z'|}-e^{-q|z+z'|})$$

and

$$k_0'=\left[k^2\mp\frac{2m^*\omega^*}{\hbar}\right]^{1/2},$$

$$q=\left[2k^2\mp\frac{2m^*\omega^*}{\hbar}-2k\left[k^2\mp\frac{2m^*\omega^*}{\hbar}\right]^{1/2}\cos\theta\right]^{1/2} .$$

Analogously, in the $Al_xGa_{1-x}As$ region

$$P^{(2)}(\mathbf{K},\mathbf{K}')=\left[\frac{2\pi e^2}{qC_2(\omega)\epsilon_0 L^2}\right]F^{(2)}_{ij}(q)\times\delta\left[\frac{\hbar^2 k'^2}{2m^*}-\frac{\hbar^2 k^2}{2m^*}\pm\hbar\omega^*\right] \quad (27)$$

and

$$P^{(2)}_{ij}(\mathbf{K})=\left[\frac{2\pi e^2 m^*}{(2\pi)^2 C_2(\omega)\epsilon_0\hbar^2}\right]\begin{bmatrix} n+1 \\ n \end{bmatrix}\times\int_0^{2\pi}d\theta\frac{F^{(2)}_{ij}(k_0',\theta)}{q} , \quad (28)$$

where

$$F^{(2)}_{ij}(q)=\int_{-\infty}^{0}\chi_j^*(z)\chi_i(z)dz\times\int_{-\infty}^{0}\chi_j^*(z')\chi_i(z')\times dz'(e^{-q|z-z'|}-e^{-q|z+z'|})$$

and

$$k_0'=\left[k^2\mp\frac{2m^*\omega^*}{\hbar}\right]^{1/2},$$

$$q=\left[2k^2\mp\frac{2m^*\omega^*}{\hbar}-2k\left[k^2\mp\frac{2m^*\omega^*}{\hbar}\right]^{1/2}\cos\theta\right]^{1/2} .$$

Figure 4(a) shows the different contributions to the emission scattering rates per unit time for the $1\rightarrow 1$ intrasubband transition within the Γ valley, compared with the GaAs bulk phonon curve. The continuous line refers to half-space LO modes characteristic of GaAs, the dashed line to the interface GaAs-like modes originating from the GaAs region, the dotted line to the interface AlAs-like modes originating from the AlAs region, and the dashed-dotted line to the GaAs-bulk phonons. The sum of the contributions of all modes characteristic of the heterostructure leads to a total probability very similar to the GaAs-bulk phonon curve. We see, moreover, that for the Al composition $x=0.3$ considered here, the contribution of the GaAs-like IF modes is about a factor 2 higher than the AlAs-like ones. The relative importance of these interface modes is a function of the Al content x, and is determined by two factors. The first is the electron-phonon polar coupling, which is stronger for AlAs-like modes than for GaAs-like ones.[11] Thus the former becomes dominant around $x=0.4$. The second factor is the phonon thermal populations. Due to the higher energy of the optical phonon, the AlAs-like population is much lower than the GaAs-like one, about a factor 2 at room temperature (0.17 versus 0.33). Since, for $x=0.3$, the square Hamiltonian (which appear in the

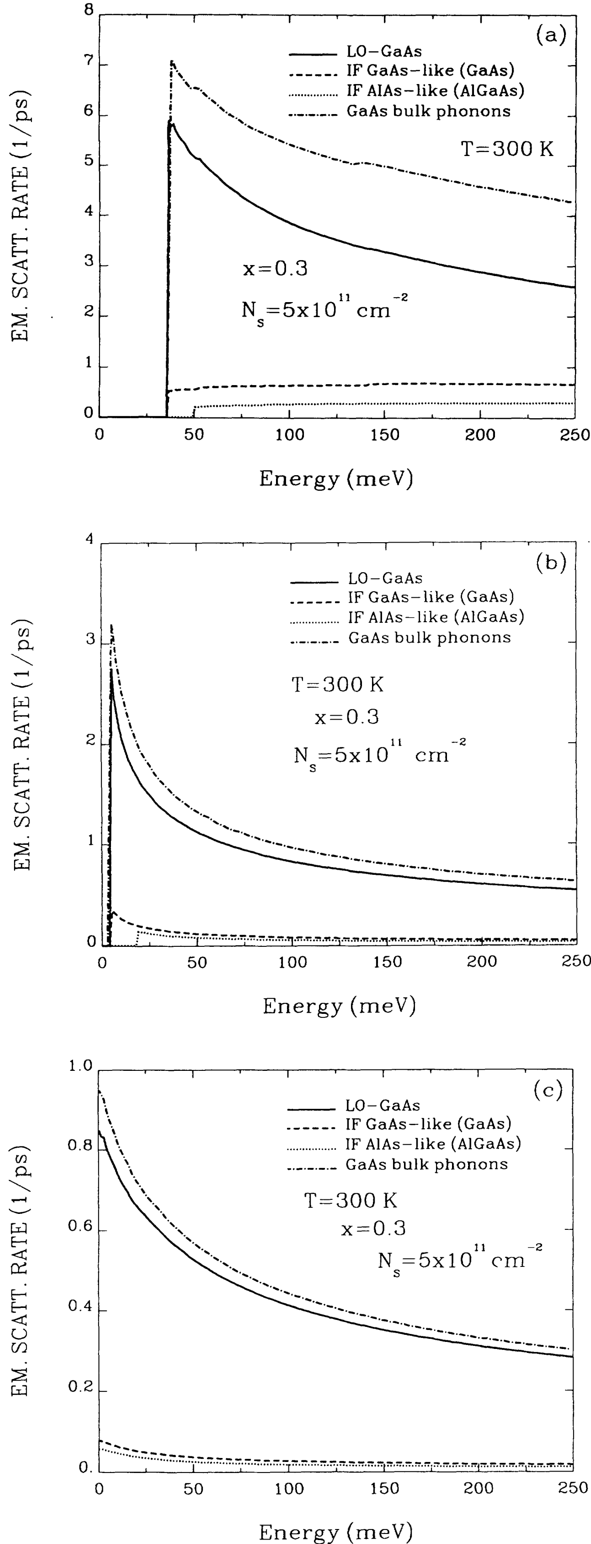

FIG. 4. (a) Phonon emission scattering rates for the intersubbands transition $1\rightarrow1$ of the Γ-valley, at 300 K, for an Al composition $x=0.3$ and a two-dimensional electron-gas concentration $N_S=5\times10^{11}$ cm^{-2}. A comparison between the modes characteristic of the system and the GaAs-bulk modes (dashed-dotted line) is shown. (b) Same as (a), for the intersubbands transition $2\rightarrow1$. (c) Same as (a), for the intersubbands transition $3\rightarrow1$.

scattering rate expression) of the interface GaAs-like modes is still slightly higher than those of the AlAs-like modes, by accounting for the different phonon populations we obtain the factor 2 mentioned above.

Figures 4(b) and 4(c) refer to the subband transitions $2\rightarrow1$ and $3\rightarrow1$, respectively, of the Γ valley. The mean features are similar to those described for the $1\rightarrow1$ transition, but in these cases the relative contribution of the interface modes is reduced, because, as seen previously, the electrons in the subbands 2 and 3 are less localized with respect to those in the ground state.

The results obtained for the first three subbands of the L valley are shown in Figures 5(a)–5(c). Here, for sake of simplicity, we have not included the GaAs-bulk phonon curve. With respect to the Γ valley, a relative increase of the contribution from interface and half-space AlAs-like modes is observed, in agreement with the wave-function analysis of Sec. II.

V. ELECTRONIC TRANSPORT IN SINGLE HETEROSTRUCTURE

The scattering rates analyzed in Sec. IV have been included in a MC code to study the transport properties of an $Al_xGa_{1-x}As$/GaAs heterojunction in the presence of an electric field applied along the heterointerface (for a comparison see Ref. 6). We have used a two-valley (Γ and L) model for both GaAs and $Al_xGa_{1-x}As$ layers, with size quantization in both valleys, as described in Sec. II. We have simulated 10 000 electrons in a standard ensemble MC scheme.[22,23] The following scattering mechanisms have been included: polar-optical phonons, ionized impurities, and the intervalley Γ-L interaction treated with deformation potential. "Real-space transfer" effects are not explicitly accounted for, the only possibility of finding carriers in the $Al_xGa_{1-x}As$ layer being a consequence of wave-function penetration in the barrier.

In principle it is necessary to update the potential profile and screening parameters as the electron distribution in the different subbands is modified in high electric fields. As already stated by Yokoyama and Hess,[6] a solution of the Schrödinger equation for each MC step require enormous computational resources, and we have therefore ignored the changes of the potential well and screening in our calculations.

Our simulation program allows us to take care of the nonequilibrium phonon population[12,23–26] by using a MC algorithm developed in recent years by the authors and co-workers.[13,14,25,27] We have performed simulations with both equilibrium and nonequilibrium phonon populations for an Al composition $x=0.3$ at 300 and 77 K. MC results are compared with experimental data by Masselink and co-workers.[28,29] Such measurements are performed by applying a superposition of a large sinusoidal electric field and a small dc electric field to the sample, and measuring the dc current as a function of the peak ac field.

Figures 6(a) and 6(b) report the drift steady-state velocity as a function of the electric field applied along with interface, at 300 and 77 K, respectively. MC curves are presented both for nonequilibrium (continuous line) and

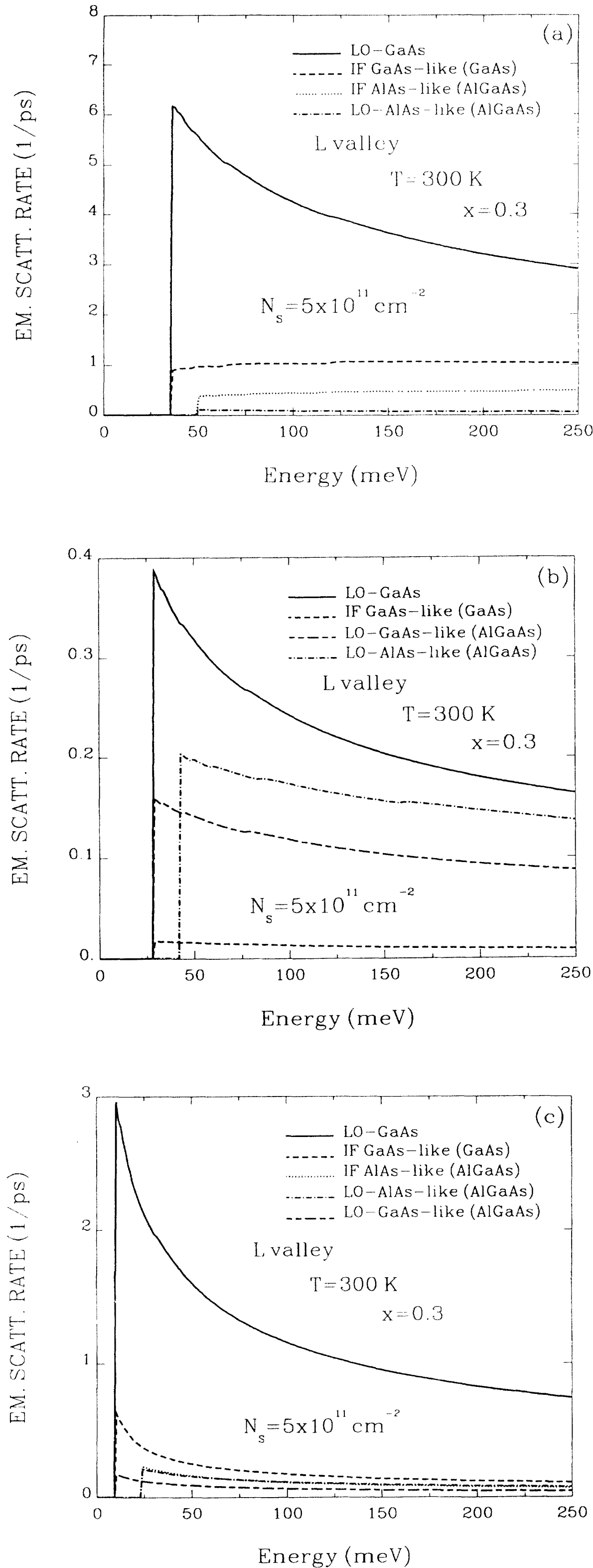

FIG. 5. (a) Phonon emission scattering rates for the intersubband transition $1 \rightarrow 1$ of the L valley, at 300 K, for an Al composition $x=0.3$ and a two-dimensional electron-gas concentration $N_S=5\times10^{11}$ cm^{-2}. Here, for sake of simplicity, the GaAs-bulk phonon curve has not been included. (b) Same as (a), for the intersubband transition $2 \rightarrow 1$. (c) Same as (a), for the intersubband transition $3 \rightarrow 1$.

equilibrium (dashed line) phonons, and compared with two sets of experimental results:[28,29] dotted lines refer to the same structure simulated by MC; dotted-dashed to the case of the lightly doped GaAs bulk with $N_D \sim 10^{15}$ cm^{-3}. At 300 K for a two-dimensional electron concentration $N_S=5\times10^{11}$ cm^{-3}, we see phonon drag and phonon heating effects.[13,14,25] Because of the nature of the polar-electron–LO-phonon scattering, the scattering probability is proportional to the inverse of the phonon wave vector. In the presence of an external electric field, the phonon population is therefore enhanced at small wave vectors in the field direction. At low fields (below 2 kV/cm) the carriers' mean energy is low enough to allow, as a consequence of energy and momentum conservation, a strong coupling with the perturbed phonon distribution, which favors the reabsorption by the electrons of those phonons with wave vectors in the direction of the electric field, leading to an increase of the drift velocity in

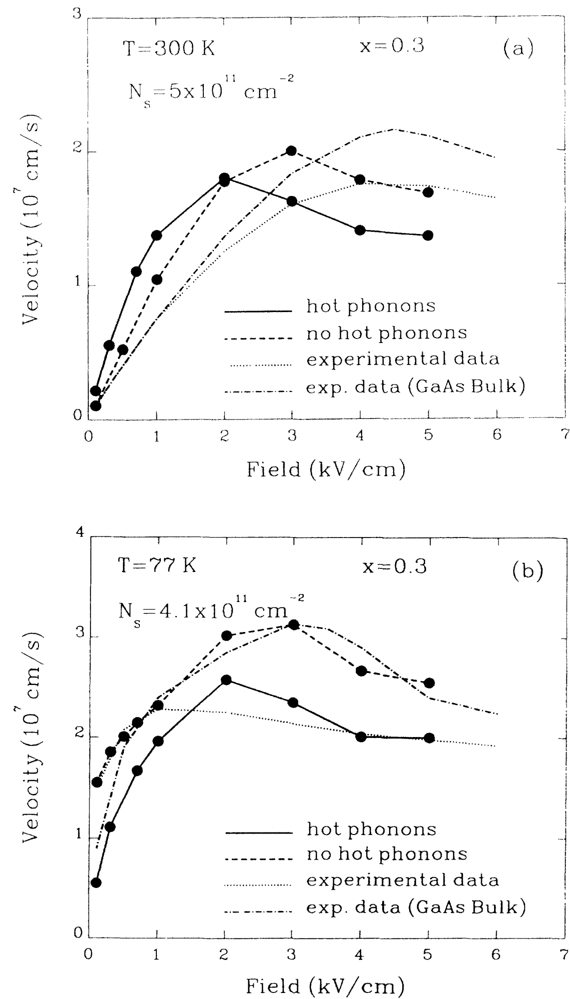

FIG. 6. Steady-state velocity vs field characteristic at (a) 300 and (b) 77 K. Comparison between Monte Carlo calculations with nonequilibrium (continuous line) and equilibrium (dashed line) phonon distributions and experimental data of Refs. 30 and 31 (dotted line). The dashed-dotted curve represents the experimental data corresponding to the undoped GaAs-bulk case.

respect to the equilibrium phonon case (drag effect[14]). With increasing field and carrier mean energy, the coupling between the carriers and the peak phonon perturbation decreases, and the electrons reabsorb mainly phonons with randomly distributed wave vectors. In this case, the dominant effect is the overall increase in the phonon population with respect to the unperturbed case, which is responsible for a larger frictional effect with a consequent reduction in the drift velocity (heating effect).

At the lattice temperature of 77 K [Fig. 6(b)], the drag regime was not detectable by our simulation. The absence of phonon drag effect for this case of higher electron mobility can be ascribed to a more dominant "phonon heating," related to a stronger frictional action of the phonon disturbances. A similar result also has been obtained in bulk GaAs.[14] In any case, all curves show an increase of velocity in respect to the room-temperature situation; this is due to the reduction of the phonon population with temperature, which implies a reduction of the electron-phonon-scattering rates.[30]

The velocity-field curves show the well-known negative differential mobility effect. This effect is due to the increase of the effective mass and consequent slowing down experienced by the carriers when they pass from the Γ to the L valley. Carriers in the Γ valley with energy higher than the Γ-L transition threshold can pass in the L valley, thus reducing their velocity. An increase in the electric field causes an increase of the carriers' mean energy. Consequently the fraction of electrons which are transferred to the L valley rises, leading to a reduction in the drift velocity.

Both at 300 and 77 K, the peak velocity of the two-dimensional electron gas is lower than that of electrons in lightly doped bulk GaAs (dashed and dotted lines) and occurs at somewhat lower electric fields. This behavior is explained through the electron size quantization in the GaAs region of the single heterostructure. In fact, since the electrons are spatially confined, the density of states is steplike with the lowest energy available for electron states coinciding with the lowest Γ- and L-valley subbands. The intervalley gap then becomes the gap between the lowest subbands of the two conduction valleys, being reduced from about 300 to about 280 meV. Since the intervalley transfer and the peak velocity depend on this energy difference in an exponential manner, the reduction of the effective valley separation plays an important role.

Figures 7 and 8 show the stationary nonequilibrium phonon distribution as a function of the bidimensional phonon wave vector q, and of the cosine of the angle which it forms with the direction of the applied field, for the half-space GaAs-like LO modes and the GaAs-like interface modes, respectively, at 300 K, for a 1-kV/cm field. The equilibrium distribution (Planck distribution), assuming no dispersion for the optical phonons, should be represented by a flat histogram, whose value at 300 K is around 0.33. As we reported above, the perturbation involves mainly phonons with small q in the electric-field direction. In Sec. III we found that, because of the shape of the phonon potential and the electron wave functions, the coupling of the carriers to the interface modes is

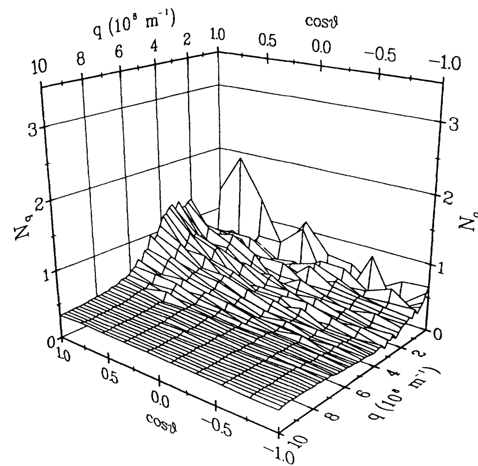

FIG. 7. Three-dimensional plot of the stationary perturbed phonon distribution for the half-space GaAs-like LO modes, as a function of the two-dimensional component $\mathbf{q}$ of the phonon wave vector and of the cosine of the angle between $\mathbf{q}$ and the electric field, at 300 K for an electric field of 1 kV/cm.

weaker than to the half-space GaAs-like LO modes. As a consequence we observe a stronger increase in the half-space LO-phonon population than in the interface modes.

This behavior becomes more evident at increasing values of the in-plane electric field. Figures 9 and 10 represent the room-temperature stationary nonequilibrium phonon population, at 3 kV/cm for the half-space GaAs-like LO modes and the GaAs-like interface modes, respectively. The perturbation in the nonequilibrium phonon population is stronger here because of the higher carriers' mean energy. The AlAs-like interface mode distribution behaves in an analogous way to the GaAs-like one. The only difference is that, because of the lower coupling between these modes and electrons discussed in Sec. IV, the perturbation intensity is sensibly reduced.

In order to increase the contribution of interface modes, it should be necessary to reduce the size of the confining well; that is, to increase the field strength along the direction perpendicular to the interface or, in other

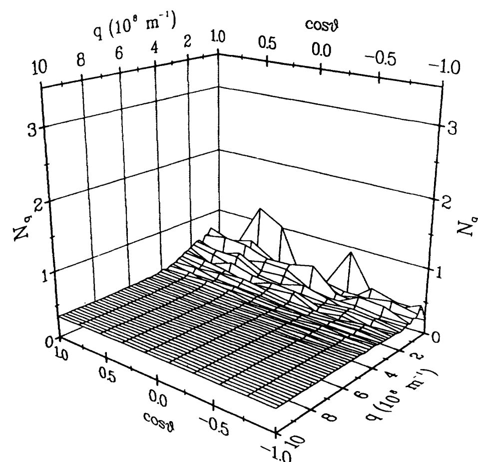

FIG. 8. Same as in Fig. 7, but for the interface modes.

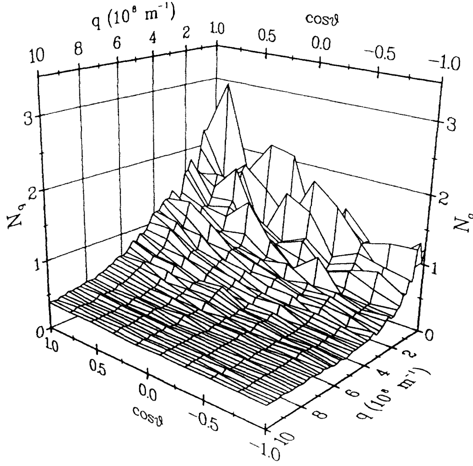

FIG. 9. Three-dimensional plot of the stationary perturbed phonon distribution for the half-space GaAs-like LO modes, as a function of the two-dimensional component **q** of the phonon wave vector and of the cosine of the angle between **q** and the electric field, at 300 K for an electric field of 3 kV/cm.

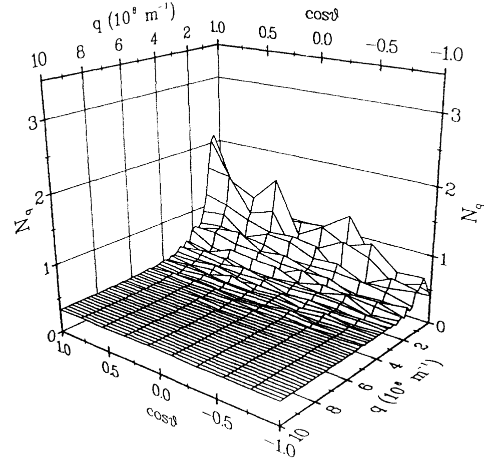

FIG. 10. Same as in Fig. 9, but for the interface modes.

words, to increase the two-dimensional electron-gas concentration. This could be achieved, for instance, by changing the gate voltage in a gated structure. A quasi-triangular quantum well like the one used in this paper is too wide (mean width about 250 Å) to observe a relevant contribution to the transport properties of the interface modes. Moreover, in Sec. III we have seen that the sum of scattering rates of modes characteristic of the system practically coincides with the GaAs bulk contribution. For these reasons we can say that, for a situation like the one analyzed in this paper, the use of GaAs bulk phonons is still a very good approximation. In fact, MC simulations performed with bulk modes have given results very similar to those presented here.[31]

VI. CONCLUSIONS

We have presented a Monte Carlo study of electronic transport in single $Al_xGa_{1-x}As$/GaAs heterostructures. A dielectric continuum model has allowed us to identify the characteristic modes of such system, which can be classified as half-space and interface modes, depending on their localization and spatial extension. The electronic wave functions, calculated by solving the coupled Schrödinger-Poisson equation, are used to evaluate the electron-phonon-scattering rates, where the phonon potential is provided by the dielectric continuum model. The MC results for the electric-field dependence of the drift velocity agree well with available experimental data obtained in modulation-doped structures. It has been shown that, depending on the width of the two-dimensional electron gas (which depends on the gate voltage for gated heterostructures), it is possible to switch the relative importance of the phonon modes from the half-space to the interface ones. Our analysis, which includes nonequilibrium phonon effects, has clearly shown the influence of the phonon perturbation, which results in both drag and heating of the drifting carriers by the perturbed phonons.

ACKNOWLEDGMENTS

Mario Gulia and Elisa Molinari are gratefully acknowledged for helpful discussions. The present work has been partially supported by the ESPRIT project NANOPT.

APPENDIX A

The interaction Hamiltonian for electrons and interface phonons in a single heterostructure was given by Eq. (19). Here we will evaluate explicitly the differential and integrated scattering rates of confined electrons with interface phonons, starting from the matrix element

$$M^I_{\mathbf{KK}'} = \langle u' | H_{epI} | u \rangle$$

appearing in the Fermi golden rule [Eq. (22)]. By writing $|u\rangle = |\mathbf{K}\rangle |n\rangle$ and from Eq. (19), we have

$$\begin{aligned} M^I_{\mathbf{KK}'} &= \langle \mathbf{K}' | \langle n \pm 1 | \left[\frac{\hbar e^2}{\epsilon_0 L^2 C_I(\omega)} \right]^{1/2} \frac{1}{\sqrt{q}} e^{-q|z|} e^{i\mathbf{q}\cdot\mathbf{r}} (\hat{a}_{\mathbf{q}} + \hat{a}^+_{-\mathbf{q}}) | n \rangle | \mathbf{K} \rangle \\ &= \left[\frac{\hbar e^2}{\epsilon_0 L^2 C_I(\omega)} \right]^{1/2} \sum_{\mathbf{q}} \langle \mathbf{K}' | \frac{1}{\sqrt{q}} e^{-q|z|} e^{i\mathbf{q}\cdot\mathbf{r}} \langle n \pm 1 | [\hat{a}_I(\mathbf{q}) + \hat{a}^+_I(-\mathbf{q})] | n \rangle | \mathbf{K} \rangle \\ &= \left[\frac{\hbar e^2}{\epsilon_0 L^2 C_i(\omega)} \right]^{1/2} \begin{Bmatrix} \sqrt{n+1} \\ \sqrt{n} \end{Bmatrix} \sum_{\mathbf{q}} \langle \mathbf{K}' | \frac{1}{\sqrt{q}} e^{-q|z|} e^{\mp i\mathbf{q}\cdot\mathbf{r}} | \mathbf{K} \rangle \ . \end{aligned}$$

The electronic wave functions for electrons confined in the z direction but free in the xy plane can be written as

$$\Psi_{\mathbf{K}}(\mathbf{R})=\zeta_i(z)e^{i\mathbf{k}\cdot\mathbf{r}} , \tag{A1}$$

where i is the subband index.

$$M^I_{\mathbf{KK}'}=\left[\frac{\hbar e^2}{\epsilon_0 L^2 C_I(\omega)}\right]^{1/2}\begin{bmatrix}\sqrt{n+1}\\ \sqrt{n}\end{bmatrix}\sum_{\mathbf{q}}\int \zeta_j^*(z)e^{-i\mathbf{k}'\cdot\mathbf{r}}\frac{e^{-q|z|}}{\sqrt{q}}e^{\mp i\mathbf{q}\cdot\mathbf{r}}\zeta_i(z)e^{i\mathbf{k}\cdot\mathbf{r}}d\mathbf{R}$$

$$=\left[\frac{\hbar e^2}{\epsilon_0 L^2 C_I(\omega)}\right]^{1/2}\begin{bmatrix}\sqrt{n+1}\\ \sqrt{n}\end{bmatrix}\sum_{\mathbf{q}}\int e^{-i(\mathbf{k}'-\mathbf{k}\pm\mathbf{q})\cdot\mathbf{r}}d\mathbf{r}\int \zeta_j^*(z)\zeta_i(z)\frac{e^{-q|z|}}{\sqrt{q}}dz .$$

Here, the integral over $\mathbf{r}$ represents the δ-Dirac function, which allows us to select the phonon wave vector $\mathbf{q}$ determined by the momentum conservation ($\mathbf{k}'-\mathbf{k}\pm\mathbf{q}=0$). By performing the sum over $\mathbf{q}$ in this way, we obtain

$$M^I_{\mathbf{KK}'}=\left[\frac{\hbar e^2}{\epsilon_0 L^2 C_I(\omega)}\right]^{1/2}\begin{bmatrix}\sqrt{n+1}\\ \sqrt{n}\end{bmatrix}\int \zeta_j^*(z)\zeta_i(z)\frac{e^{-q|z|}}{\sqrt{q}}dz , \tag{A2}$$

$$|M^I_{\mathbf{KK}'}|^2=\left[\frac{\hbar e^2}{\epsilon_0 L^2 C_I(\omega)}\right]\begin{bmatrix}n+1\\ n\end{bmatrix}\frac{1}{q}G^I_{ij}(q) , \tag{A3}$$

where

$$G^I_{ij}(q)=\int \zeta_j^*(z)\zeta_i(z)e^{-q|z|}dz\int \zeta_j^*(z')\zeta_i(z')e^{-q|z'|}dz' .$$

The transition rate from electronic state $\mathbf{K}$ to $\mathbf{K}'$ is

$$P^I(\mathbf{K},\mathbf{K}')=\frac{2\pi}{\hbar}|M^I_{\mathbf{KK}'}|^2\delta(E_f-E_{\text{in}})$$

which, together with Eq. (A3), gives directly the expression of Eq. (23), with

$$E_f=\frac{\hbar^2k'^2}{2m^*}+E_j\pm\hbar\omega,\quad E_{\text{in}}=\frac{\hbar^2k^2}{2m^*}+E_i .$$

The argument of the δ function is written as

$$\frac{\hbar^2k'^2}{2m^*}-\frac{\hbar^2k^2}{2m^*}\pm\hbar\omega^* ,$$

where $\pm\hbar\omega^*=\pm\hbar\omega+(E_j-E_i)$. The total probability that an electron in the state $|\mathbf{K}\rangle$ performs a transition assisted by an interface phonon is given by

$$P^I_{ij}(\mathbf{k})=\frac{L^2}{(2\pi)^2}\int P(\mathbf{k}i,\mathbf{k}'j)d\mathbf{k}'$$

$$=\frac{L^2}{(2\pi)^2}\frac{2\pi}{\hbar}\left[\frac{\hbar e^2}{\epsilon_0 L^2 C_I(\omega)}\right]\begin{bmatrix}n+1\\ n\end{bmatrix}\int\frac{G^I_{ij}(q)}{q}\delta\left[\frac{\hbar^2k'^2}{2m^*}-\frac{\hbar^2k^2}{2m^*}\pm\hbar\omega^*\right]d\mathbf{k}'$$

$$=\frac{e^2}{2\pi\epsilon_0 C_I(\omega)}\begin{bmatrix}n+1\\ n\end{bmatrix}\int\frac{G^I_{ij}(q)}{q}\delta\left[\frac{\hbar^2k'^2}{2m^*}-\frac{\hbar^2k^2}{2m^*}\pm\hbar\omega^*\right]d\mathbf{k}' .$$

By writing $q=\sqrt{k'^2+k^2-2kk'\cos\theta}$ and passing to polar coordinates, we have

$$P^I_{ij}=\frac{e^2}{2\pi\epsilon_0 C_i(\omega)}\begin{bmatrix}n+1\\ n\end{bmatrix}\int_0^{2\pi}d\theta\int_0^{\infty}G^I_{ij}(k',\theta)\frac{\delta\left[\frac{\hbar^2k'^2}{2m^*}-\frac{\hbar^2k^2}{2m^*}\pm\hbar\omega^*\right]}{\sqrt{k'^2+k^2-2kk'\cos\theta}}k'dk' .$$

The integral over $\mathbf{k}'$ can be performed analytically by using the energy-conserving δ function. The final result is

$$P_{ij}^{I}(\mathbf{k})=\frac{m^{*}e^{2}}{2\pi\hbar^{2}\epsilon_{0}C_{I}(\omega)}\begin{bmatrix}n+1\\ n\end{bmatrix}\int_{0}^{2\pi}\frac{G_{ij}^{I}(k',\theta)}{\sqrt{k_{0}'^{2}+k^{2}-2kk_{0}'\cos\theta}}d\theta\ , \tag{A4}$$

where

$$k_{0}'=\left[k^{2}\mp\frac{2m^{*}\omega^{*}}{\hbar}\right]^{1/2} .$$

APPENDIX B

1. Binary semiconductor

The interaction Hamiltonian for the half-space LO mode in a binary semiconductor is given by Eq. (20). By following the same procedure as in Appendix A, the matrix element

$$\begin{aligned}M_{\mathbf{KK}'}^{(1)}&=-\langle\mathbf{K}'|\langle n+1|\sum_{q_z>0}\sum_{\mathbf{q}}\left[\frac{\hbar e^{2}\omega_{L1}}{2\epsilon_{0}L^{3}}\right]^{1/2}\left[\frac{1}{\epsilon_{\infty1}}-\frac{1}{\epsilon_{1}(0)}\right]^{1/2}\frac{e^{i\mathbf{q}\cdot\mathbf{r}}}{\sqrt{q^{2}+q_{z}^{2}}}2\sin(q_{z}z)[\hat{a}_{1,qz}(\mathbf{q})+\hat{a}_{1,qz}^{+}(-\mathbf{q})]|n\rangle|\mathbf{K}\rangle\\&=-\left[\frac{4\hbar e^{2}\omega_{L1}}{2\epsilon_{0}L^{3}}\right]^{1/2}\left[\frac{1}{\epsilon_{\infty1}}-\frac{1}{\epsilon_{1}(0)}\right]^{1/2}\begin{bmatrix}\sqrt{n+1}\\ \sqrt{n}\end{bmatrix}\sum_{q_z>0}\sum_{\mathbf{q}}\langle\mathbf{K}'|\frac{e^{i\mathbf{q}\cdot\mathbf{r}}}{\sqrt{q^{2}+q_{z}^{2}}}\sin(q_{z}z)|\mathbf{K}\rangle\end{aligned}$$

can be written explicitly as

$$\begin{aligned}M_{\mathbf{KK}'}^{(1)}&=-\left[\frac{4\hbar e^{2}\omega_{L1}}{2\epsilon_{0}L^{3}}\right]^{1/2}\left[\frac{1}{\epsilon_{\infty1}}-\frac{1}{\epsilon_{1}(0)}\right]^{1/2}\begin{bmatrix}\sqrt{n+1}\\ \sqrt{n}\end{bmatrix}\sum_{q_z>0}\sum_{\mathbf{q}}\int\zeta_{j}^{*}(z)e^{-i\mathbf{k}'\cdot\mathbf{r}}\frac{e^{\mp i\mathbf{q}\cdot\mathbf{r}}}{\sqrt{q^{2}+q_{z}^{2}}}\sin(q_{z}z)\zeta_{i}(z)e^{i\mathbf{k}\cdot\mathbf{r}}d\mathbf{R}\\&=-\left[\frac{4\hbar e^{2}\omega_{L1}}{2\epsilon_{0}L^{3}}\right]^{1/2}\left[\frac{1}{\epsilon_{\infty1}}-\frac{1}{\epsilon_{1}(0)}\right]^{1/2}\begin{bmatrix}\sqrt{n+1}\\ \sqrt{n}\end{bmatrix}\sum_{q_z>0}\sum_{\mathbf{q}}\int e^{-i(\mathbf{k}'-\mathbf{k}\pm\mathbf{q})\cdot\mathbf{r}}d\mathbf{r}\int_{0}^{\infty}\zeta_{j}^{*}(z)\zeta_{i}(z)\frac{\sin(q_{z}z)}{\sqrt{q^{2}+q_{z}^{2}}}dz\ .\end{aligned}$$

Once again the integral over $\mathbf{r}$ represents the δ function $\delta(\mathbf{k}'-\mathbf{k}\pm\mathbf{q})$ for momentum conservation, which allows us to perform the sum over $\mathbf{q}$ and obtain

$$|M_{\mathbf{KK}'}^{(1)}|^{2}=\left[\frac{4\hbar e^{2}\omega_{L1}}{2\epsilon_{0}L^{3}}\right]\left[\frac{1}{\epsilon_{\infty1}}-\frac{1}{\epsilon_{1}(0)}\right]\begin{bmatrix}n+1\\ n\end{bmatrix}\times\sum_{q_z>0}\frac{G_{ij}^{(1)}(q_{z})}{q^{2}+q_{z}^{2}}\ ,$$

where

$$G_{ij}^{(1)}(q_{z})=\int_{0}^{\infty}\zeta_{j}^{*}(z)\zeta_{i}(z)\sin(q_{z}z)dz\times\int_{0}^{\infty}\zeta_{j}^{*}(z')\zeta_{i}(z')\sin(q_{z}z')dz'\ .$$

By using the same transformation of the δ function as in Appendix A, for the differential scattering rate we have

$$P_{ij}^{(1)}(\mathbf{k},\mathbf{k}')=\frac{2\pi}{\hbar}\left[\frac{\hbar e^{2}\omega_{L1}}{2\epsilon_{0}L^{3}}\right]\left[\frac{1}{\epsilon_{\infty1}}-\frac{1}{\epsilon_{1}(0)}\right]\begin{bmatrix}n+1\\ n\end{bmatrix}\times\sum_{q_z>0}\frac{G_{ij}^{(1)}(q_{z})}{q^{2}+q_{z}^{2}}\delta\left[\frac{\hbar^{2}k'^{2}}{2m^{*}}-\frac{\hbar^{2}k^{2}}{2m^{*}}\pm\hbar\omega^{*}\right] .$$

By converting the sum over q_z into an integral in q_z [$\sum_{q_z>0}\Longrightarrow(L/\pi)\int_{0}^{\infty}dq_z$], we have

$$P_{ij}^{(1)}(\mathbf{k},\mathbf{k}')=\left[\frac{e^{2}\omega_{L1}}{\epsilon_{0}L^{2}}\right]\left[\frac{1}{\epsilon_{\infty1}}-\frac{1}{\epsilon_{1}(0)}\right]\begin{bmatrix}n+1\\ n\end{bmatrix}\times\int_{0}^{\infty}\frac{G_{ij}^{(1)}(q_{z})}{q^{2}+q_{z}^{2}}dq_{z}\times\delta\left[\frac{\hbar^{2}k'^{2}}{2m^{*}}-\frac{\hbar^{2}k^{2}}{2m^{*}}\pm\hbar\omega^{*}\right] .$$

We define the "form factor" $A_{ij}^{(1)}(q)$ as

$$\begin{aligned}A_{ij}^{(1)}(q)&=\int_{0}^{\infty}\frac{G_{ij}^{(1)}(q_{z})}{q^{2}+q_{z}^{2}}dq_{z}\\&=\int_{0}^{\infty}\zeta_{j}^{*}(z)\zeta_{i}(z)dz\times\int_{0}^{\infty}\zeta_{j}^{*}(z')\zeta_{i}(z')dz'\times\int_{0}^{\infty}\frac{4\sin(q_{z}z)\sin(q_{z}z')dz'}{q^{2}+q_{z}^{2}}dq_{z}\ .\end{aligned}$$

The integral on the far right,

$$I=4\int_{0}^{\infty}\frac{4\sin(q_{z}z)\sin(q_{z}z')dz'}{q^{2}+q_{z}^{2}}dq_{z}\ ,$$

can be put in the form

$$I=-\int_{-\infty}^{\infty}\frac{e^{iq_z(z+z')}}{q^2+q_z^2}dq_z+\int_{-\infty}^{\infty}\frac{e^{iq_z(z-z')}}{q^2+q_z^2}dq_z$$

and solved with the residue method, to give in our case[32]

$$I=\frac{\pi}{q}(e^{-q|z-z'|}-e^{-q|z+z'|}) .$$

Thus

$$A_{ij}^{(1)}(q)=\frac{\pi}{q}\int_0^{\infty}\zeta_j^*(z)\zeta_i(z)dz \times\int_0^{\infty}\zeta_j^*(z')\zeta_i(z')dz'(e^{-q|z-z'|}-e^{-q|z+z'|})$$

and

$$P_{ij}^{(1)}(\mathbf{k},\mathbf{k}')=\left[\frac{\pi e^2\omega_{L1}}{\epsilon_0 L^2 q}\right]\left[\frac{1}{\epsilon_{\infty 1}}-\frac{1}{\epsilon_1(0)}\right] \times\begin{bmatrix}n+1\\ n\end{bmatrix}F_{ij}^{(1)}(q)\delta\left[\frac{\hbar^2k'^2}{2m^*}-\frac{\hbar^2k^2}{sm^*}\pm\hbar\omega^*\right], \quad \text{(B1)}$$

where, for sake of simplicity, we have set $A_{ij}^{(1)}(q)=F_{ij}^{(1)}(q)(\pi/q)$. The total scattering rate is

$$P_{ij}^{(1)}(\mathbf{k})=\frac{L^2}{(2\pi)^2}\int P^{(1)}(\mathbf{k}i,\mathbf{k}'j)d\mathbf{k}'\left[\frac{\pi e^2\omega_{L1}}{(2\pi)^2\epsilon_0}\right]\left[\frac{1}{\epsilon_{\infty 1}}-\frac{1}{\epsilon_1(0)}\right]\begin{bmatrix}n+1\\ n\end{bmatrix}\int\frac{F_{ij}^{(1)}(q)}{q}\delta\left[\frac{\hbar^2k'^2}{2m^*}-\frac{\hbar^2k^2}{2m^*}\pm\hbar\omega^*\right]d\mathbf{k}' \quad \text{(B2)}$$

which leads to Eq. (26) after transformation to polar coordinates and integration of the $\mathbf{k}'$ integral.

2. Ternary semiconductor

The interaction Hamiltonian is given by Eq. (21). The functional form of this Hamiltonian is the same of that of the binary semiconductor. Therefore calculations are performed in the same way, changing only the coefficients, and remembering that ω can assume other one of the two values ω_{L2A} and ω_{L2G}:

$$P_{ij}^{(2)}(\mathbf{k},\mathbf{k}')=\frac{2\pi}{\hbar}\left[\frac{\hbar e^2}{C_2(\omega)\epsilon_0 L^3}\right]\begin{bmatrix}n+1\\ n\end{bmatrix} \times\sum_{q_z>0}\frac{G_{ij}^{(2)}(q_z)}{q^2+q_z^2}\delta\left[\frac{\hbar^2k'^2}{2m^*}-\frac{\hbar^2k^2}{2m^*}\pm\hbar\omega^*\right],$$

$$G_{ij}^{(2)}(q_z)=\int_{-\infty}^{0}\zeta_j^*(z)\zeta_i(z)2\sin(q_z z)dz \times\int_{-\infty}^{0}\zeta_j^*(z')\zeta_i(z')2\sin(q_z z')dz' .$$

By transforming the sum over q_z into an integral, we obtain

$$P_{ij}^{(2)}(\mathbf{k},\mathbf{k}')=\left[\frac{2e^2}{C_2(\omega)\epsilon_0 L^2}\right]\begin{bmatrix}n+1\\ n\end{bmatrix} \times\int_0^{\infty}\frac{G_{ij}^{(2)}(q_z)}{q^2+q_z^2}dq_z \times\delta\left[\frac{\hbar^2k'^2}{2m^*}-\frac{\hbar^2k^2}{2m^*}\pm\hbar\omega^*\right].$$

In this case the form factor is given by

$$A_{ij}^{(2)}(q)=\int_0^{\infty}\frac{G_{ij}^{(2)}(q_z)}{q^2+q_z^2}dq_z =\int_{-\infty}^{0}\zeta_j^*(z)\zeta_i(z)dz \times\int_{-\infty}^{0}\zeta_j^*(z')\zeta_i(z')dz' \times\int_0^{\infty}\frac{4\sin(q_z z)\sin(q_z z')dz'}{q^2+q_z^2}dq_z .$$

The integral over q_z has already been evaluated for the binary semiconductor; here we give only the final result:

$$A_{ij}^{(2)}(q)=\frac{\pi}{q}\int_{-\infty}^{0}\zeta_j^*(z)\zeta_i(z)dz \times\int_{-\infty}^{0}\zeta_j^*(z')\zeta_i(z')dz' \times(e^{-q|z-z'|}-e^{-q|z+z'|}) ,$$

from which Eq. (27) follows immediately, where the notation $A_{ij}^{(2)}(q)=F_{ij}^{(2)}(q)(\pi/q)$ is used. Analogously to the binary semiconductor case, the total scattering rate of Eq. (28) is calculated through the integration over all final states.

---

*Present address: Center for Solid State Electronics Research, Arizona State University, Tempe, AZ 85287-6206.

[1] *Microwave and Millimeter-Wave Heterostructures Transistors and Their Applications*, edited by F. Ali, I. Bahl, and A. Gupta (Artech House, Norwood, VA, 1989).
[2] *Low Dimensional Structures in Semiconductors*, edited by A. R. Peaker and H. G. Grimmeiss (Plenum, New York, 1991).
[3] R. Dingle, H. L. Stormer, A. C. Gossard, and W. Weigmann,

Appl. Phys. Lett. **33**, 665 (1978).

[4]H. L. Stormer, J. Phys. Soc. Jpn. Suppl. A. **49**, 1013 (1980).

[5]G. Bastard, *Wave Mechanics Applied to Semiconductor Heterostructures* (Les Éditions de Physique, Paris, 1990).

[6]K. Yokoyama and K. Hess, Phys. Rev. B **33**, 5595 (1986).

[7]R. Fuchs and K. L. Kliewer, Phys. Rev. **140**, A2076 (1965).

[8]L. Wendler and R. Pechstedt, Phys. Status Solidi B **141**, 129 (1987).

[9]N. Mori and T. Ando, Phys. Rev. B **40**, 6175 (1989).

[10]H. Rücker, E. Molinari, and P. Lugli, Phys. Rev. B **45**, 6747 (1992).

[11]K. W. Kim and M. A. Stroscio, J. Appl. Phys. **68**, 6289 (1990).

[12]P. Kocevar, Physica **134B**, 155 (1985).

[13]P. Lugli, P. Bordone, L. Reggiani, M. Rieger, P. Kocevar, and S. M. Goodnick, Phys. Rev. B **39**, 7852 (1989).

[14]M. Rieger, P. Kocevar, P. Lugli, P. Bordone, L. Reggiani, and S. M. Goodnick, Phys. Rev. B **39**, 7866 (1989).

[15]F. Stern and S. Das Sarma, Phys. Rev. B **30**, 840 (1984).

[16]T. Ando, J. Phys. Soc. Jpn. **51**, 3893 (1982).

[17]B. Vinter, Solid State Commun. **48**, 151 (1983).

[18]B. Vinter, Appl. Phys. Lett. **44**, 307 (1984).

[19]S. Adachi, J. Appl. Phys. **58**, R1 (1985).

[20]H. Haken, *Quantum Field Theory of Solids* (North-Holland, Amsterdam, 1976).

[21]J. J. Licari and R. Evrard, Phys. Rev. B **15**, 2254 (1977).

[22]C. Jacoboni and P. Lugli, *The Monte Carlo Method for Semiconductor Device Simulation* (Springer-Verlag, Wien, 1989).

[23]S. M. Goodnick and P. Lugli, in *Hot Carriers in Semiconductors,* edited by J. Shah (Academic, New York, 1992), p. 191.

[24]P. Kocevar, Phys. Status Solidi B **84**, 681 (1977); P. Kocevar and E. Fitz, *ibid.* **89**, 225 (1978).

[25]P. Bordone, C. Jacoboni, P. Lugli, L. Reggiani, and P. Kocevar, J. Appl. Phys. **61**, 1460 (1987).

[26]P. Kocevar, *Festkörperprobleme (Advances in Solid State Physics),* edited by P. Grosse (Pergamon, New York, 1987), Vol. 27, p. 197.

[27]P. Lugli, Solid-State Electron. **31**, 667 (1988).

[28]W. T. Masselink, N. Braslau, W. I. Wang, and S. L. Wright, Appl. Phys. Lett. **51**, 1533 (1987).

[29]W. T. Masselink, Semicond. Sci. Technol. **4**, 503 (1989).

[30]We do not expect that the inclusion of real-space transfer would lead to major changes in our results. In fact, the spatial transfer of electrons into the $Al_xGa_{1-x}As$ layer occurring at high fields is already accounted for (although in an indirect way) by the extended wave functions of the L valley.

[31]We do not report the results obtained with bulk GaAs phonon modes, because they do not differ from those presented here within the accuracy of the MC method.

[32]S. M. Goodnick and P. Lugli, Phys. Rev. B **37**, 2578 (1988).